Numer. Math. Theor. Meth. Appl.
doi: 10.4208/nmtma.2009.m9001s

Vol. **2**, No. 4, pp. 353-376
November 2009

A Compound Algorithm of Denoising Using Second-Order and Fourth-Order Partial Differential Equations

Qianshun Chang[1], Xuecheng Tai[2,3] and Lily Xing[1,*]

[1] *Institute of Applied Mathematics, Academy of Mathematics and Systems Sciences, Chinese Academy of Sciences, Beijing, China.*
[2] *School of Physical and Mathematical Sciences, Nanyang Technological University, SPMS-04-01, 21 Nanyang Link, Singapore 637371.*
[3] *Department of Mathematics, University of Bergen, Johannes Brunsgate 12, 5008 Bergen, Norway.*

Received 8 February 2009; Accepted (in revised version) 6 June 2009

Abstract. In this paper, we propose a compound algorithm for the image restoration. The algorithm is a convex combination of the ROF model and the LLT model with a parameter function θ. The numerical experiments demonstrate that our compound algorithm is efficient and preserves the main advantages of the two models. In particular, the errors of the compound algorithm in L_2 norm between the exact images and corresponding restored images are the smallest among the three models. For images with strong noises, the restored images of the compound algorithm are the best in the corresponding restored images. The proposed algorithm combines the fixed point method, an improved AMG method and the Krylov acceleration. It is found that the combination of these methods is efficient and robust in the image restoration.

AMS subject classifications: 68U10, 65M55

Key words: Algorithm of denoising, image restoration, total variation, second-order functional.

1. Introduction

Image restoration is an important problem with numerous applications in both image processing and medical problems. The image restoration is to recover original images from noisy and blurred data. Mathematically, image restoration is to recover the true image u from the observed image z by the formula

$$z = Ku + n, \tag{1.1}$$

where K is a known linear blurring operator and n is a Gaussian white noise.

*Corresponding author. *Email addresses:* qschang@amss.ac.cn (Q. Chang), tai@mi.uib.no (X. Tai), xinglily@amss.ac.cn (L. Xing)

In recent years, many models for noise removal and deblurring are proposed and studied. One of the basic models is the total variation based restoration method proposed by Rudin, Osher and Fatemi [18]. In this model, the following total variation minimization problem is considered:

$$\min_u \left(\alpha \int_\Omega |\nabla u| \, dxdy + \frac{1}{2}\|Ku - z\|_{L^2}^2 \right), \tag{1.2}$$

where $|\nabla u| = \sqrt{u_x^2 + u_y^2}$ and $\alpha > 0$ is the penalty parameter.

The corresponding Euler-Lagrange equation for (1.2) is

$$-\alpha \nabla \cdot \left(\frac{\nabla u}{|\nabla u|} \right) + K^*(Ku - z) = 0, \quad \text{in } \Omega, \tag{1.3}$$

where K^* is the adjoint operator of K with respect to standard L_2 inner product. This idea gives a rigorous mathematical tool to introduce nonlinear diffusion filters in the image restoration. Motivated by the total variation norm, many similar models of restoration are proposed in literatures (see [2,3,6,12,13,15,22,23]).

In these papers, several papers (see [6, 12, 13, 15, 22, 23]) discuss the noise removal methods by fourth-order partial differential equations. Especially, Lysaker, Lundervold and Tai in [13] proposed a problem of second-order functional minimization by the formula

$$\min_u \left(\alpha \int_\Omega |D^2 u| \, dxdy + \frac{1}{2}\|Ku - z\|_{L^2}^2 \right), \tag{1.4}$$

where

$$|D^2 u| = \sqrt{u_{xx}^2 + u_{xy}^2 + u_{yx}^2 + u_{yy}^2}.$$

The corresponding Euler-Lagrange equation for (1.4) is

$$\alpha \left\{ \left(\frac{u_{xx}}{|D^2 u|} \right)_{xx} + \left(\frac{u_{xy}}{|D^2 u|} \right)_{yx} + \left(\frac{u_{yx}}{|D^2 u|} \right)_{xy} + \left(\frac{u_{yy}}{|D^2 u|} \right)_{yy} \right\} + K^*(Ku - z) = 0, \quad \text{in } \Omega. \tag{1.5}$$

It is known that the higher-order PDEs can recover smoother surfaces. In dealing with higher-order PDEs, a major challenge is to pursue the quality in (1.2) along jumps. However, it seems to be difficult to use one algorithm to preserve discontinuities in one part of the image and simultaneously recover smooth signals in other parts. Hence, combining different algorithms remains a possible approach to improve the image restoration capability. In [6, 12, 15], authors discuss the methods of combining both a lower- and a higher-order PDE.

The ROF model (1.2) is known to be better than LLT model (1.4) when denoising and identifying locations of discontinuities and amplitude of jumps. In another side, the LLT model is better than ROF model in handling smooth signals and keeping small constructions and shapes of the images. In [15], Lysaker and Tai use the convex combination of the solutions of (1.2) and (1.4) to get better restoration images (see [15]).

In this paper we propose a new combination algorithm of the model (1.2) and the model (1.4) on the basis of idea of [15]. By analyzing underlying features in the interesting image, we combine the formulae (1.2) and (1.4) with a variable parameter θ.

Section 2 of this paper describes the combination algorithm. The discretization formulae of our model are given in Section 3. The algorithms of the denoising problems and methods of accelerating convergence are discussed in Section 4. Section 5 is devoted to numerical experiments. Finally, some conclusions are discussed in Section 6.

2. New combination algorithm

We consider a convex combination of the models (1.2) and (1.4):

$$\min_u \left[\alpha \left(\int_\Omega \theta |\nabla u| \, dxdy + \int_\Omega (1-\theta)|D^2 u| \, dxdy \right) + \frac{1}{2}\|Ku - z\|_{L^2}^2 \right], \tag{2.1}$$

where θ is a variable parameter which will be given later.

The corresponding Euler-Lagrange equation for (2.1) is very complicated, because θ is dependent with $|\nabla u|$. In this model, the θ is only a variable parameter and is applied to control combination of the ROF model (1.2) and the LLT model (1.4). Therefore, we present the following simplified iterative model:

$$\min_{u^{s+1}} \left[\alpha \left(\int_\Omega \theta^s |\nabla u^{s+1}| \, dxdy + \int_\Omega (1-\theta^s)|D^2 u^{s+1}| \, dxdy \right) + \frac{1}{2}\|Ku^{s+1} - z\|_{L^2}^2 \right], \tag{2.2}$$

where initial guess u^0 is given as the observed image z, then θ^s, $s = 0, 1, \cdots$ are computed by u^s and new iterative value u^{s+1} is solved from the minimization problem (2.2).

The corresponding Euler-Lagrange equation for (2.2) is

$$\begin{aligned} \alpha \Bigg\{ \Bigg[\Big(\frac{(1-\theta^s)u_{xx}^{s+1}}{|D^2 u^{s+1}|}\Big)_{xx} + \Big(\frac{(1-\theta^s)u_{xy}^{s+1}}{|D^2 u^{s+1}|}\Big)_{yx} + \Big(\frac{(1-\theta^s)u_{yx}^{s+1}}{|D^2 u^{s+1}|}\Big)_{xy} + \Big(\frac{(1-\theta^s)u_{yy}^{s+1}}{|D^2 u^{s+1}|}\Big)_{yy} \Bigg] \\ - \Bigg[\Big(\frac{\theta^s u_x^{s+1}}{|Du^{s+1}|}\Big)_x + \Big(\frac{\theta^s u_y^{s+1}}{|Du^{s+1}|}\Big)_y \Bigg] \Bigg\} + K^*(Ku^{s+1} - z) = 0, \quad \text{in } (0,1)^2, \end{aligned} \tag{2.3}$$

where

$$\begin{aligned} |D^2 u| &= \sqrt{(u_{xx})^2 + (u_{xy})^2 + (u_{yx})^2 + (u_{yy})^2}, \\ |Du| &= \sqrt{(u_x)^2 + (u_y)^2}. \end{aligned}$$

In our convex combination, the second-order PDE is used when $|\nabla u|$ is small or large. Thus, the noise may be removed in the smooth region and edges can be detected in the discontinuities. In the same time, the fourth-order PDE is applied when $|\nabla u|$ is middle such that the small constructions and shapes of the images are kept.

3. Choice of the variable parameter θ

For the compound algorithm, the variable parameter θ is important. We choose broken lines for the θ:

$$\theta = \begin{cases} 1, & \text{if } |\nabla u| \leqslant C_0 \text{ and } |\nabla u| \geqslant C_1, \\ C_d, & \text{if } C_0 + 5 \leq |\nabla u| \leq C_1 - 5, \\ 1 - \dfrac{(|\nabla u| - C_d)(1 - C_d)}{5} & \text{if } C_0 \leq |\nabla u| \leq C_0 + 5, \\ 1 + \dfrac{(|\nabla u| - C_1)(1 - C_d)}{5} & \text{if } C_1 - 5 \leq |\nabla u| \leq C_1. \end{cases} \tag{3.1}$$

The curve of θ are given in Fig. 1.

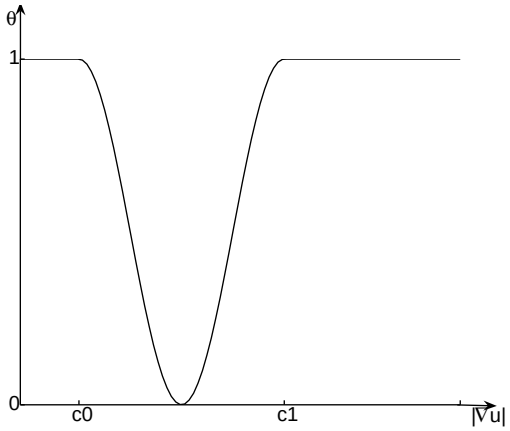

Figure 1: Curve of θ.

In computation, the parameters $C_0 = 0$, and $C_d = 0.1$ are fixed. The parameter C_1 is taken as 40 for the most images and is properly modificated for some images.

Thus, the 4-th order equation is used mainly in middle domain of $|\nabla u|$ such that the smoothness of image can be kept. ROF model is applied when $|\nabla u|$ is large or small. Thus, denoising image has clear edges and noise can be removed efficiently.

4. Discretization formulae

The nonlinear partial differential equation (2.3) is applied to restorate the images. Eq. (2.3) is discretized by the difference methods. The all terms of Eq. (2.3) are approximated by the corresponding divided central difference.

We use the average of adjacent values to give the values which are not restored on the

grid:

$$u^{s+1}_{i-1/2,j} = \frac{1}{2}(u^{s+1}_{i,j} + u^{s+1}_{i-1,j}),$$
$$u^{s+1}_{i+1/2,j+1/2} = \frac{1}{4}(u^{s+1}_{i,j} + u^{s+1}_{i+1,j} + u^{s+1}_{i,j+1} + u^{s+1}_{i+1,j+1}),$$
$$(u_{i,j})_x = \frac{1}{h}(u_{i,j+1} - u_{i,j}), \quad (u_{i,j})_{\bar{x}} = \frac{1}{h}(u_{i,j} - u_{i,j-1}),$$

where $u_{i,j}$ is located in the center of cell, h denotes the step size of space and $h = 1/I$, I is total number of points in one direction (x-direction or y-direction).

Thus, the discretized nonlinear algebraic system of equations can be written in the form:

$$\alpha\Bigg\{\Bigg[\Big(\frac{(1-\theta^s)(u^{s+1}_{i,j})_{x\bar{x}}}{D^{2(s+1)}_{i,j}}\Big)_{x\bar{x}} + \Big(\frac{(1-\theta^s)(u^{s+1}_{i,j})_{xy}}{D^{2(s+1)}_{i+1/2,j+1/2}}\Big)_{\bar{y}\bar{x}} + \Big(\frac{(1-\theta^s)(u^{s+1}_{i,j})_{yx}}{D^{2(s+1)}_{i+1/2,j+1/2}}\Big)_{\bar{x}\bar{y}}$$
$$+ \Big(\frac{(1-\theta^s)(u^{s+1}_{i,j})_{y\bar{y}}}{D^{2(s+1)}_{i,j}}\Big)_{y\bar{y}}\Bigg] - \Bigg[\Big(\frac{\theta^s(u^{s+1}_{i,j})_x}{D^{(s+1)}_{i+1/2,j}}\Big)_{\bar{x}} + \Big(\frac{\theta^s(u^{s+1}_{i,j})_y}{D^{(s+1)}_{i,j+1/2}}\Big)_{\bar{y}}\Bigg]\Bigg\} + K^*(Ku^{s+1}_{i,j} - z_{i,j}) = 0,$$
$$i = 1, \cdots I, \quad j = 1, \cdots J \quad (I = J), \tag{4.1}$$

where

$$(D^{2(s+1)}_{i,j})^2 = \frac{1}{h^4(1-\theta^s_{i,j})^2}\Bigg[\Big((u^{s+1}_{i,j})_{x\bar{x}}\Big)^2 + \Big((u^{s+1}_{i,j})_{y\bar{y}}\Big)^2$$
$$+ 2\Big(u^{s+1}_{i+1/2,j+1/2} + u^{s+1}_{i-1/2,j-1/2} - u^{s+1}_{i-1/2,j+1/2} - u^{s+1}_{i+1/2,j-1/2}\Big)^2\Bigg], \tag{4.2}$$

and

$$(D^{(s+1)}_{i+1/2,j})^2$$
$$= \frac{1}{h^2(\theta^s_{i+1/2,j})^2}\Bigg[\Big(u^{s+1}_{i+1,j} - u^{s+1}_{i,j}\Big)^2 + \frac{1}{16}\Big(u^{s+1}_{i+1,j+1} + u^{s+1}_{i,j+1} - u^{s+1}_{i+1,j-1} - u^{s+1}_{i,j-1}\Big)^2\Bigg]. \tag{4.3}$$

In real computations, the numerical boundary conditions are important and should be chosen carefully. We consider and compare many numerical boundary conditions in numerical experiments. The following two boundary conditions with the truncation error of order 2 are simple and efficient for the image restoration:

1. Neumann boundary condition

$$u_{0,j} = u_{1,j}, \quad u_{i,0} = u_{i,1}, \quad u_{I+1,j} = u_{I,j}, \quad u_{i,J+1} = u_{i,J}. \tag{4.4}$$

2. Continuity boundary condition, which is an extrapolation formula of order 2

$$\begin{aligned} u_{-1,j} &= 3u_{1,j} - 2u_{2,j}, & u_{i,-1} &= 3u_{i,1} - 2u_{i,2}, \\ u_{I+2,j} &= 3u_{I,j} - 2u_{I-1,j}, & u_{i,J+2} &= 3u_{i,J} - 2u_{i,J-1}. \end{aligned} \tag{4.5}$$

The system of algebraic equations is very complicated and strong nonlinear. Especially, the denominators $D_{i,j}^{2(s+1)}$ and $D_{i+1/2,j}^{(s+1)}$ are possible to equal zero.

5. Algorithms of denoising problems and methods of accelerating convergence

In this paper, we only consider denoising problems. Hence, the blurring operator K is given as identity operator.

In order to avoid that the denominators equal to zero, the a small quantity β is added to the terms $D_{i,j}^{4(s+1)}$ and $D_{i+1/2,j}^{2(s+1)}$.

5.1. Fixed point method

The system of nonlinear equations (4.1), (4.4) and (4.5) is solved by the fixed point method (see [20, 21]), i.e., the $u_{i,j}$ in all denominators take sth approximations values of the solution. The computational formulae are

$$\alpha\Bigg\{\Bigg[(\frac{(1-\theta^s)(u_{i,j}^{s+1})_{x\bar{x}}}{D_{i,j}^{2(s)}})_{x\bar{x}}+(\frac{(1-\theta^s)(u_{i,j}^{s+1})_{xy}}{D_{i+1/2,j+1/2}^{2(s)}})_{\bar{y}\bar{x}}+(\frac{(1-\theta^s)(u_{i,j}^{s+1})_{yx}}{D_{i+1/2,j+1/2}^{2(s)}})_{\bar{x}\bar{y}}$$
$$+(\frac{(1-\theta^s)(u_{i,j}^{s+1})_{yy}}{D_{i,j}^{2(s)}})_{\bar{y}\bar{y}}\Bigg]-\Bigg[(\frac{\theta^s(u_{i,j}^{s+1})_{x}}{D_{i+1/2,j}^{(s)}})_{\bar{x}}+(\frac{\theta^s(u_{i,j}^{s+1})_{y}}{D_{i,j+1/2}^{(s)}})_{\bar{y}}\Bigg]\Bigg\}+K^*(Ku_{i,j}^{s+1}-z_{i,j})=0,$$
$$i=1,\cdots I,\quad j=1,\cdots J\quad (I=J). \tag{5.1}$$

The equations (4.1) for new approximation $u_{i,j}^{s+1}$ are a linear algebraic system when the values $u_{i,j}^{s}$ are known and are solved by our algebraic multigrid (AMG) method.

Thus, the equations (4.1) with the boundary conditions (4.4) and (4.5) are solved by two-level iterations: (i) outer iteration of the fixed poind method from $u_{i,j}^{s}$ to $u_{i,j}^{s+1}$; and (ii) inner iteration of the AMG method to obtain $u_{i,j}^{s+1}$ when $u_{i,j}^{s}$ are known.

The convergence of the fixed point method is slow. We apply Krylov subspace algorithm to accelerate convergence of the nonlinear iteration (see [16]).

5.2. Basic algebraic multigrid (AMG) method

The AMG method is developed to solve large systems of linear equations using the principles of usual multigrid method (see [8–10, 19]). In the AMG method, there are two phases: setup phase and solving phase.

Now, we describe our version of the AMG algorithm [10, 19] briefly. We consider the following $n \times n$ system of linear equations

$$AU = F. \tag{5.2}$$

An AMG method breaks this equation into a sequence of smaller and smaller equations: $A^m U^m = F^m$, $m = 1, \cdots, M$, where $A^m = (a^m_{i,j})_{n_m \times n_m}$, $U^m = (u^m_1, u^m_2, \cdots, u^m_{n_m})^T$, and $F^m = (f^m_1, f^m_2, \cdots, f^m_{n_m})^T$, with $n = n_1 > n_2 > \cdots > n_M$, $A^1 = A, U^1 = U, F^1 = F$. These equations formally play the same role as the coarse grid equations in the GMG method.

In a standard multigrid process, one needs to define the coarse grids, the interpolation operator I^m_{m+1}, the restriction operator I^{m+1}_m, and the coarse grid operator A^{m+1}. With these, at each level, a smoothing process, say Gauss-Seidel, is applied to the equation $A^m U^m = F^m$ to find an approximate solution $\widehat{U}^m$. The high frequency errors of the residual $r^m := F^m - A^m \widehat{U}^m$ are usually reduced in this smoothing process. The correction for low frequency errors is approximated by the following procedure. First, the correction equation $A^m e^m = r^m$ is restricted to the next coarser grid by the restriction operator. The resulting equation is solved to obtain the coarse grid correction e^{m+1}. This correction e^{m+1} is then interpolated back to level m by the interpolation operator to obtain approximate solution e^m.

We shall adopt Galerkin type algorithm, where $I^{m+1}_m = (I^m_{m+1})^T$ and $A^{m+1} = I^{m+1}_m A^m I^m_{m+1}$. Thus, we will only need to define the coarse grids and interpolation operators. We follow the approach in [10, 19] to define the grid Ω^m and its coarse grid C^m. The grid Ω^m is regarded as the indices $\{1, \cdots, n_m\}$ of the unknowns e^m_j, $1 \le j \le n_m$. The coarse grid C^m is a subset of Ω^m. The grid Ω^{m+1} is nothing but a re-indexing of C^m. We denote $\Omega^m - C^m$ by F^m, the fine grid. Criteria to determine C^m will be discussed later.

The interpolation operator I^m_{m+1} maps data on Ω^{m+1} to data on Ω^m. Namely, for $i \in C^m$, the datum e^m_i is taken to be the datum on the corresponding index on Ω^{m+1}; while for $i \in F^m$, e^m_i is interpolated from data on C^m. Roughly speaking, this interpolation formula is derived so that the i^{th} equation

$$a^m_{i,i} e^m_i + \sum_{j \in N^m_i} a^m_{i,j} e^m_j = r^m_i \approx 0 \tag{5.3}$$

is almost satisfied. Here,

$$N^m_i = \left\{ j \in \Omega^m \mid a^m_{i,j} \neq 0,\ j \neq i \right\},$$

which can be thought as the neighbors of i.

In order to solve (5.3) approximately, we classify the neighbors of the point i into two classes. A point $j \in N^m_i$ is said to be strongly connected to i if

$$\mid a^m_{i,j} \mid \ge \theta \cdot \max_{k \neq i} \mid a^m_{i,k} \mid$$

for some fixed $0 < \theta \le 1$, and weakly connected if otherwise. We denote the collection of these neighboring points by S^m_i (strong) and W^m_i (weak), respectively. We also denote $C^m \bigcap S^m_i$ by C^m_i. Our goal is to derive an interpolation formula

$$e^m_i = \sum_{j \in C^m_i} \omega_{i,j} e^m_j, \quad \text{for } i \in F^m$$

so that the i^{th} correction equation is almost satisfied:

$$a_{i,i}^m e_i^m + \sum_{j \in N_i^m} a_{i,j}^m e_j^m = 0. \tag{5.4}$$

Note that $N_i^m = S_i^m \cup W_i^m = (S_i^m \cap C^m) \cup (S_i^m \cap F^m) \cup W_i^m$. The issue here is how to approximate e_j^m with $j \in S_i^m \cap F^m$ or $j \in W_i^m$ in terms of e_i or e_k^m with $k \in C_i^m$. Before going to the discussion of this issue, let us describe how to choose the coarse grid C^m for a moment.

The coarse grid C^m is chosen such that the following criteria are satisfied:

(C1) For each point $i \in F^m$, every point $j \in S_i^m$ is either in C_i^m or strongly connected to at least one point in C_i^m (i.e. $S_j^m \cap C_i^m \neq \varphi$).

(C2) C^m should be the maximal subset of all points with the property that any two points in C^m are not strongly connected to each other.

Condition (C1) ensures that for $i \in F^m$, e_i^m can be constructed from the values e_k^m with $k \in C_i^m$ with certain accuracy. Condition (C2) means that C^m is chosen as smaller as possible to gain efficiency. In general, it is difficult to construct C^m to satisfy (C2) strictly. Ruge and Stüben [19] provided an $\mathcal{O}(n_m)$ algorithm to construct the coarse grid C^m which is small enough and leads to linear computational complexity of the overall algorithm practically.

Let us go back to the issue: how to approximate e_j^m with $j \in S_i^m \cap F^m$ or $j \in W_i^m$ in terms of e_i^m or e_k^m with $k \in C_i^m$? For $j \in W_i^m$, we may simply approximate e_j^m by

$$e_j^m = e_i^m, \tag{5.5}$$

based on the smoothness of e^m which we do expect. For $j \in S_i^m \cap F^m$, we look into the j^{th} equation:

$$a_{j,j}^m e_j^m + \sum_{k \in C_i^m \cap N_j^m} a_{j,k}^m e_k^m + \cdots \approx 0.$$

The part "$\cdots$" is secondary error and thus negligible. A natural approximation of e_j^m is the following average formula:

$$e_j^m = \sum_{k \in C_i^m \cap N_j^m} g_{j,k}^m e_k^m, \quad g_{j,k}^m = \frac{|a_{j,k}^m|}{\sum_{\ell \in C_i^m \cap N_j^m} |a_{j,\ell}^m|}. \tag{5.6}$$

The condition (C1) (i.e. $C_i^m \cap S_j^m \neq \varphi$) guarantees that $\sum_{k \in C_i^m} |a_{j,k}^m|$ is not too small. The above interpolation formula was given by J. Ruge and K. Stüben [19].

An improved interpolation formula using some geometric assumptions was proposed in [10]. It further uses an average or extrapolation of formulae (5.5) and (5.6), depending on the "relative locations" of points j, i and $\{k | k \in C_i^m \cap S_j^m\}$. These "geometric" assumptions are as below.

(G1) Elements in N_i^m are the neighbors of a point i in Ω^m. Further, the larger the quantity $|a_{i,j}^m|$ is, the closer the point j is to the point i.

(G2) If $a_{i,j}^m < 0$ or $|a_{i,j}^m|$ is small, we say that the error between i and j is geometrically smooth. Otherwise, we call it geometrically oscillating. Here, we have normalized $a_{i,i} > 0$.

Roughly speaking,"geometrically," the average location of points in $C^m \cap S_i^m \cap S_j^m$ is somewhere between i and j. Therefore the error e_j^m can be approximated more accurately by an extrapolation formula using e_i and $\sum_{k\in C_i^m\cap S_j^m} g_{j,k}e_k^m$. More precisely, let us define

$$\zeta_{i,j}^m = \frac{-\sum\limits_{k\in C_i^m\cap N_j^m} a_{j,k}^m}{\sum\limits_{k\in C_i^m\cap N_j^m} |\, a_{j,k}^m\,|}, \quad \eta_{i,j}^m = \frac{|\, a_{i,j}^m\,|}{\dfrac{1}{|C_i^m\cap N_j^m|}\sum\limits_{k\in C_i^m\cap N_j^m} |\, a_{j,k}^m\,|}.$$

The quantity $\zeta_{i,j}^m$ indicates whether there is a large negative entry $a_{j,k}^m$ for $k \in C_i^m \cap N_j^m$. When $\zeta \geq 1/2$ and $a_{i,j}^m < 0$, it can be shown that the errors between the point i and the point j are geometrically smooth. The quantity $\eta_{i,j}^m$ roughly gives the "inverse ratio" of the distance between j and i to the average distance between the point j and the points in $C_i^m \cap N_j^m$. If $\eta_{i,j}^m < 3/4$, we think the "average location" of the points in $C_i^m \cap N_j$, denoted by $\bar{k}_{j,i}$, is closer to j than that of i. That is, $\bar{k}_{j,i}$ lies between i and j, and thus, an extrapolation formula for e_j in terms of e_i and $\sum_{k\in C_i^m\cap N_j^m} g_{j,k}e_k^m$ can be applied. When $\eta_{i,j}^m > 2$, we think i is closer to j than that of $\bar{k}_{j,i}$. In this case, we use an interpolation formula instead. Otherwise, we think $\bar{k}_{j,i}$ is very close to j and we should just use the average formula $\sum_{k\in C_i^m\cap N_j^m} g_{j,k}e_k^m$ to approximate e_j.

In summary, we use the following "geometric" interpolation formulae.

(1) For $j \in S_i^m \cap F^m$, we have

$$e_j^m = \begin{cases} 2\sum_{k\in C_i^m} g_{j,k}^m e_k^m - e_i^m, & \text{if } \eta_{i,j}^m < 3/4, \zeta_{i,j} \geq 1/2 \text{ and } a_{i,j}^m < 0, \\ \frac{1}{2}(\sum_{k\in C_i^m} g_{j,k}^m e_k^m + e_i^m), & \text{if } \eta_{i,j}^m > 2, \zeta_{i,j}^m \geq 1/2 \text{ and } a_{i,j}^m < 0, \\ \sum_{k\in C_i^m} g_{j,k}^m e_k^m, & \text{otherwise.} \end{cases} \tag{5.7}$$

(2) For $j \in W_i^m$, we have

$$e_j^m = \begin{cases} e_i^m, & \text{if } C_i^m \cap S_j^m = \varphi,\ a_{i,j}^m < 0, \\ -e_i^m, & \text{if } C_i^m \cap S_j^m = \varphi,\ a_{i,j}^m > 0, \\ 2\sum_{k\in C_i^m} g_{j,k}^m e_k^m - e_i^m, & \text{if } C_i^m \cap S_j^m \neq \varphi,\ \zeta_{i,j}^m \geq 1/2 \text{ and } a_{i,j}^m < 0, \\ \sum_{k\in C_i^m} g_{j,k}^m e_k^m, & \text{otherwise.} \end{cases} \tag{5.8}$$

The convergence proof for this improved AMG method was given in [8] when A^m is symmetric positive definite. Many numerical examples also support the improvement of this "geometric" interpolation formula [10].

5.3. Krylov acceleration

Usually, the Krylov subspace method is applied in solving systems of linear equations. In [16], Oosterlee and Washio use the Krylov subspace method to solve nonlinear problem. We have used the Krylov subspace method in image denoising and deblurring problems (see [7, 11]). In this paper, the Krylov subspace method is applied to accelerate convergence of the fixed point method.

First, we choose two parameters $\bar{K}$ and s, with $\bar{K} \leq s$. The Krylov subspace acceleration is performed after every s steps of fixed point iterations as the follows. For integer $n > 0$, let

$$U^{new} = U^{ns} + \sum_{k=1}^{\bar{K}} \eta_k (U^{ns+1-k} - U^{ns-k}). \tag{5.9}$$

where the coefficients η_k are chosen such that the residual R^{new} for U^{new} is minimum in L_2 norm, i.e.,

$$\min_{\eta_1,\cdots,\eta_{\bar{K}}} (||R^{new}||^2_{L_2}). \tag{5.10}$$

The minimization problem can be equivalent to a system of linear equations for the $\eta_,\eta_,\cdots,\eta_{\bar{K}}$, which is solved to get the coefficients $\eta_,\eta_,\cdots,\eta_{\bar{K}}$. Then, We reset U^{ns} to be U^{new}.

In this paper, we combine the fixed point method, AMG method and the Krylov subspace method to solve the nonlinear equations (5.1).

6. Discussion on computation

In this section, we discuss some details related to the computations.

6.1. Normalized residual

An important issue in image restorations is to choose a quantity to measure the quality of improvement. It is used as a stopping criterion for the fixed point iteration. Usually, the residual of the system (5.1) is chosen. But, the diffusion coefficient is very large in smooth region and is relatively small in region where u is less smooth. The ratio between maximum and minimum diagonal entries is more than 10^6. Hence, a normalization is needed.

In this paper, we use $D^{-1}(Re)$ as the normalized residual. Here, (Re) is the residual of the system (5.1) and D is the corresponding diagonal matrix of system. A normalization will cure this imbalance. Numerical experiments below demonstrate that this quantity is able to measure the improvement of the denoising process. From now on, we shall denote this normalized residual by Re.

6.2. Inner iteration of AMG method

When the $u_{i,j}^s$ are obtained, the linear system (4.1) with boundary conditions (4.4) and (4.5) is a linear algebraic system. But, the system (4.1), (4.4) and (4.5) does not possess diagonal dominance, because the terms of partial differentials of the order 4.

In computation, the AMG method is efficient to solve the system (4.1), (4.4) and (4.5). The convergence factor of V-cycle of the AMG method is about 0.07. Therefore, in each outer iteration of fixed point, only one V-cycle of the AMG method is applied for solving the corresponding linear system. There is no need to have more iteration because the dominant error is from the outer iteration.

6.3. Improvement of the fixed point method by the Krylov acceleration

The slow convergence of the fixed point iteration can further be improved by the Krylov acceleration method. In the application of Krylov acceleration, we choose the parameter $s = 4$, i.e., we apply the Krylov acceleration every four fixed point iterations. The parameter K is taken to be 2, i.e., Krylov subspace algorithm with two parameters α_1 and α_2 is applied.

The numerical computation demonstrates that the total number of iterations is reduced to about 30%. The overhead is low, because only simple algebraic operations are needed. The results demonstrate that the Krylov acceleration method is very efficient to accelerate the convergence of our fixed point method.

6.4. Stopping criterion

The stopping criterion for the fixed point iteration in this paper is a relative decrease of the residual by a factor of ε, namely,

$$\frac{\|Re^N\|_{L_2}}{\|Re^0\|_{L_2}} \leq \varepsilon. \tag{6.1}$$

It is necessary to adjust the stopping criterion according to noisy level and the initial residual. The reason is that quantity of the restoration images depends on proper number of iteration. Some of the noises is kept in the restoration images if the number of iterations is too small. Some of small structures in the images are smeared if the number of iterations is too large.

In general, ε is taken as $5.0 * 10^{-3} \sim 10^{-4}$. The ε is smaller for images with the strong noise, because the initial residuals are larger in this case. When the noise is weaker or initial residual is smaller, ε is taken as $5.0 * 10^{-3}$.

In our computation, the stopping tolerance $\varepsilon = 2.0 * 10^{-4} \sim 5.0 * 10^{-3}$, when the compound algorithm is applied. For ROF model, $\varepsilon = 10^{-4}$, because convergence is fast. For the 4-th order model, $\varepsilon = 5 * 10^{-4} \sim 10^{-4}$, because denoising needs lager number of iteration and convergence is slow. The general principle is that the tolerance ε is chosen such that denoising images have high quality.

6.5. Signal-to-noise ratio (SNRT)

For an exact image u and the observed image z, the SNRT is computed by

$$SNRT = \frac{||u - \overline{u}||_{L_2}}{||(z-u) - \overline{(z-u)}||_{L_2}},$$

where

$$\overline{u} = \frac{1}{|\Omega|}\int_{\Omega} u dx dy$$

and $|\Omega|$ denoted the area of the domain Ω.

The variance of Gaussian noise σ will be listed in our tables, because the variance is an important index and SNRT has many different definitions.

7. Numerical experiments

In the numerical experiments below, we take the blur operator K to be the identity matrix. First, two benchmark images are considered here $[3, 5]$. Then, several practical images are denoised. In all images, each pixel has value in $[0, 255]$.

In computation, the parameter $\beta = 10^{-24}$ is taken, and value of α is dependent with intensity of noise and model. For ROF model, $\alpha = 0.2 \sim 1.2$. The values of α are between 0.001 and 1.0 for 4-th order model. The compound model has the smaller values of α than ones of ROF model, and $\alpha = 0.2 \sim 1.1$. A Gaussian distribution with mean 0 and variance σ is added to the original images.

In numerical experiments, we compare results of the equation of order 2, (1.3) and the equation of order 4, (1.5) with the ones of new compound equation (2.3).

In all tables to be presented in this section, N denotes number of iteration of the fixed point method, Err2 and Err0 denote errors in L_2 and L_∞ norm between exact image and restored image, respectively. CPU time is the computational time required to satisfy given residual condition (5.1).

All computation is done in a PC computer of model "Lenovo" with double cores and 2.33 GHz.

7.1. Two benchmark images

First, we test the denoising problems for the two benchmark images, the original images are given in Fig. 2. The resolution of these images are 256*256.

7.1.1. The image of two intensities with weak noise

The results of the equation of order 2, (1.3) and the equation of order 4, (1.5) and the new compound equation (2.3) are given in Table 1.

The noising image, restorated image of model of the second-order equation, restorated image of model of the fourth-order equation, and restorated image of model of the compound equation for the image of two intensities are shown in Fig. 3.

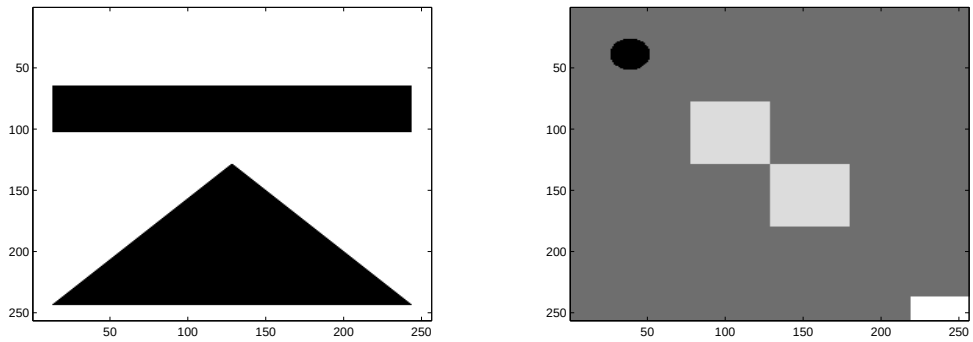

Figure 2: Original images: two colors (left), four colors (right).

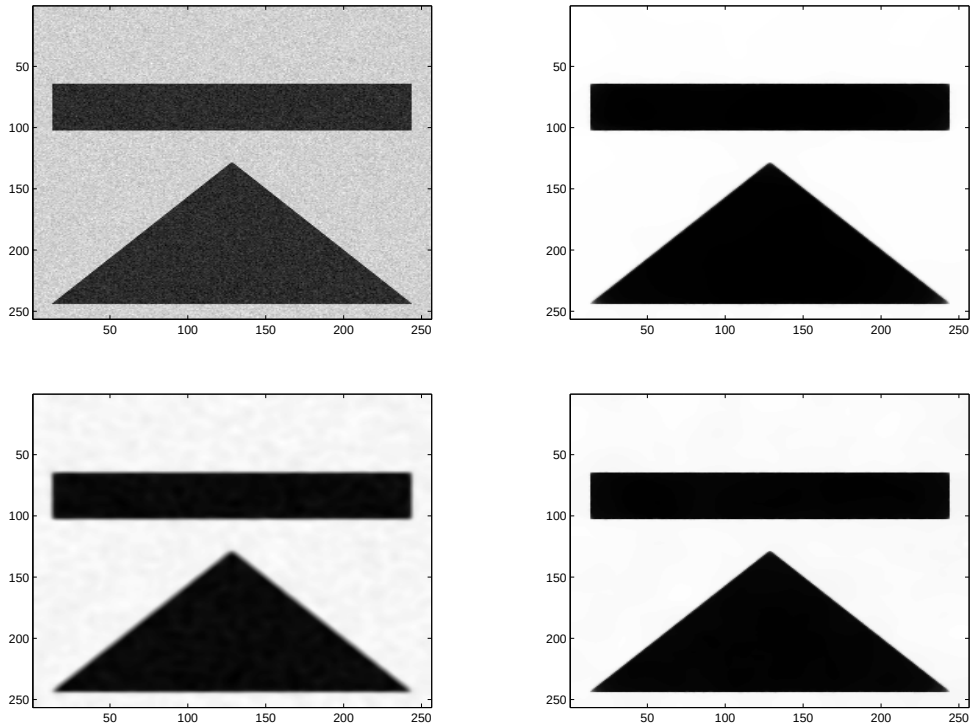

Figure 3: Noising image (up left), restored image of model of the second-order equation (up right), restored image of model of the fourth-order equation (down left), and restored image of model of the compound equation (down right) for the image of two intensities, and $\sigma = 10$, SNRT$= 6.66$.

7.1.2. The image of two intensities with strong noise

Now, we consider a denoising problem with strong noise for the image of two intensities. The results and figures of the three models are in Table 2 and Fig. 4.

Table 1: Computational results for the image of two intensities and $\sigma = 10$, SNRT$= 6.66$.

Model	ε	N	Err2	Err0	CPU time
Equation of order 2	1.0^{-3}	6	3.46	107.41	2.37
Equation of order 4	1.0^{-3}	12	9.92	109.83	8.74
Compound equation	1.0^{-3}	11	3.08	96.23	7.31

Table 2: Computational results for the image of two intensities, and $\sigma = 65$, SNRT$= 1.02$.

Model	ε	N	Err2	Err0	CPU time
Equation of order 2	$2 * 1.0^{-4}$	9	9.54	133.16	3.64
Equation of order 4	$2 * 1.0^{-4}$	24	15.42	118.36	18.10
Compound equation	$2 * 1.0^{-4}$	23	7.76	126.24	13.48

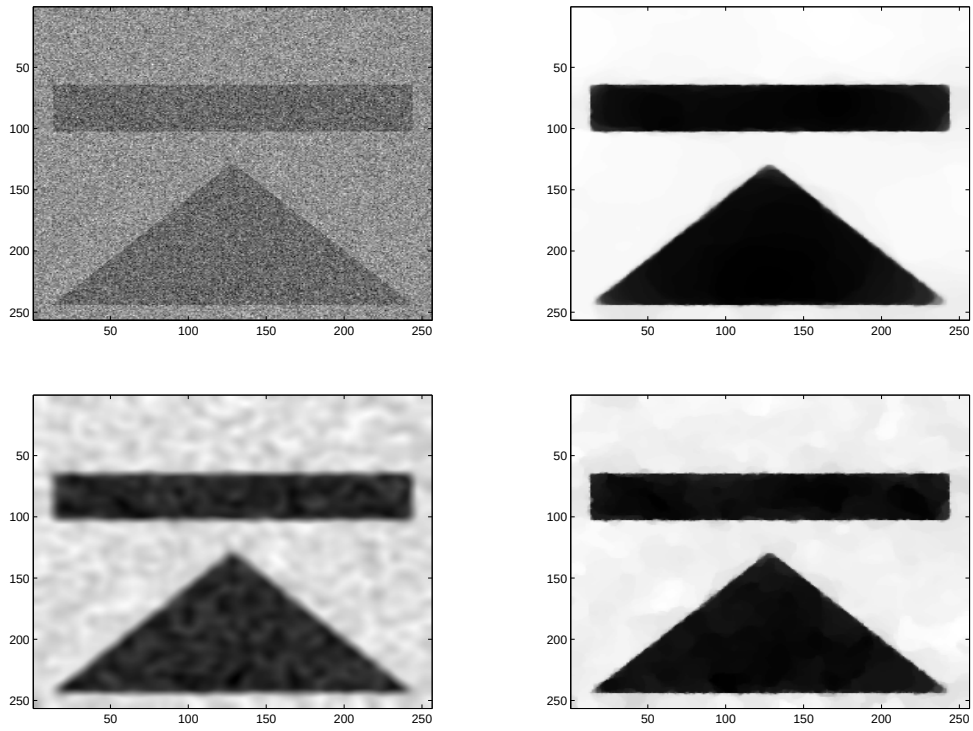

Figure 4: Noising image (up left), restored image of model of the second-order equation (up right), restored image of model of the fourth-order equation (down left), and restored image of model of the compound equation (down right) for the image of two intensities, and $\sigma = 65$, SNRT$= 1.02$.

7.1.3. The image of four colors with weak noise

A denoising problem with weak noise for the image of four colors is considered in this subsection. The computational results and figures of the three models are in Table 3 and Fig. 5.

Table 3: Computational results for the image of four colors, and $\sigma = 10$, SNRT$= 3.50$.

Model	ε	N	Err2	Err0	CPU time
Equation of order 2	1.0^{-3}	5	1.76	58.81	1.95
Equation of order 4	1.0^{-3}	10	5.74	88.55	7.04
Compound equation	1.0^{-3}	8	1.58	51.33	5.17

Table 4: Computational results for the image of four colors, and $\sigma = 40$, SNRT$= 0.87$.

Model	ε	N	Err2	Err0	CPU time
Equation of order 2	$5.0^{1}.0{-}4$	8	5.34	117.42	3.13
Equation of order 4	$5 * 1.0^{-4}$	25	6.87	91.57	18.04
Compound equation	$5 * 1.0^{-4}$	10	3.87	84.13	5.54

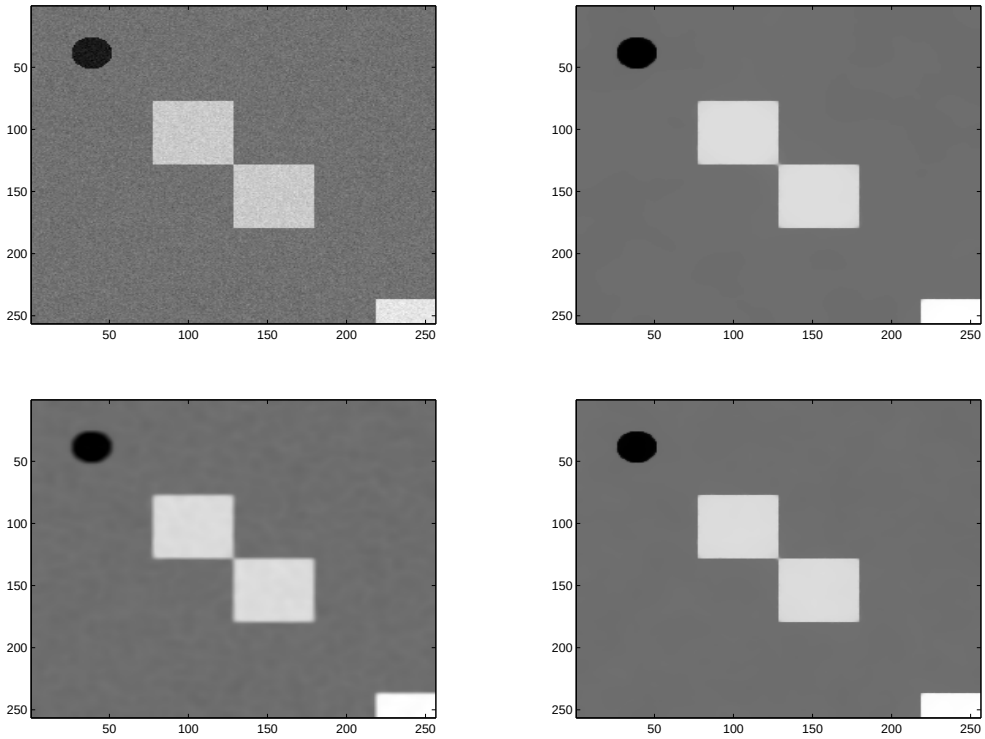

Figure 5: Noising image (up left), restored image of model of the second-order equation (up right), restored image of model of the fourth-order equation (down left), and restored image of model of the compound equation (down right) for the image of four colors, and $\sigma = 10$, SNRT$= 3.50$.

7.1.4. The image of four colors with strong noise

A denoising problem with stronger noise for the image of four colors is considered. The computational results and figures of the three models are in Table 4 and Fig. 6.

From the two benchmark images, we know that all three models can restored the

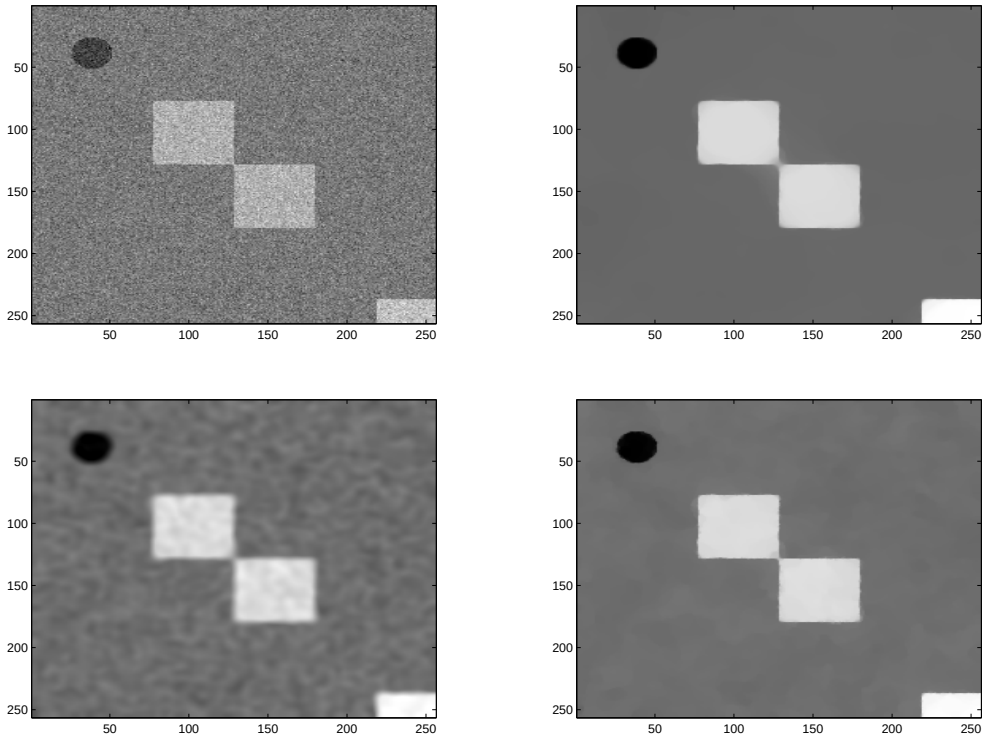

Figure 6: Noising image (up left), restored image of model of the second-order equation (up right), restored image of model of the fourth-order equation (down left), and restored image of model of the compound equation (down right) for the image of four colors, and $\sigma = 40$, SNRT$= 0.87$.

noising images when the noise is weak.

For images with strong noise, the ROF model may remove noise very well, but, smear sharp angles. The model of 4-th order equation can keep sharp angles, but, is difficult to remove stronger noise.

IN summary, the new compound algorithm has advantages of the two models, i.e., it can remove stronger noise and keep sharp angles.

7.2. Lena face image

Now, we consider the denoising problems for Lena face image. The Lena face image has been considered in many papers and its original image is given in Fig. 7. The resolution of this image is 51*51.

In the Lane face image, the parameter $C_1 = 255$ is used, because there is no strong discontinuity in this image.

In Fig. 7, we also plot the contour for image of Lena face.

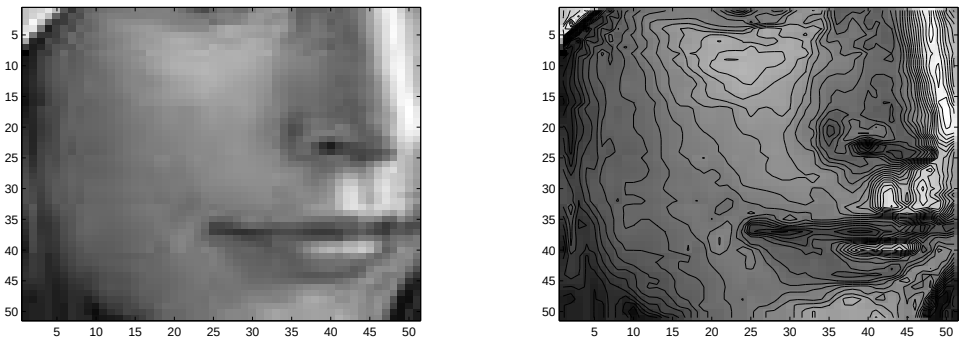

Figure 7: Original image (left) and the contour of Lena face (right).

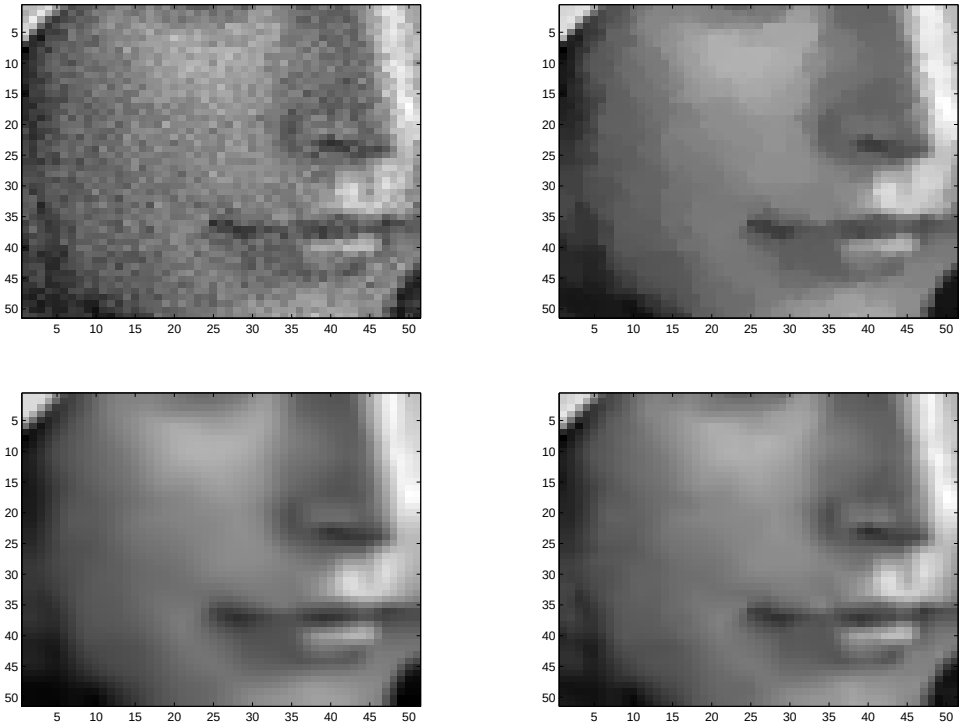

Figure 8: Noising image (up left), restored image of model of the second-order equation (up right), restored image of model of the fourth-order equation (down left), and restored image of model of the compound equation (down right) for the image of Lena face, and $\sigma = 13$, SNRT$= 3.26$.

7.2.1. The image of Lena face with weak noise

The Lena face image with weak noise has been considered in [15], p.13. The results of the three models are given in Table 5 and Fig. 8. The contour for recovered images of Lena face is presented in Fig. 9.

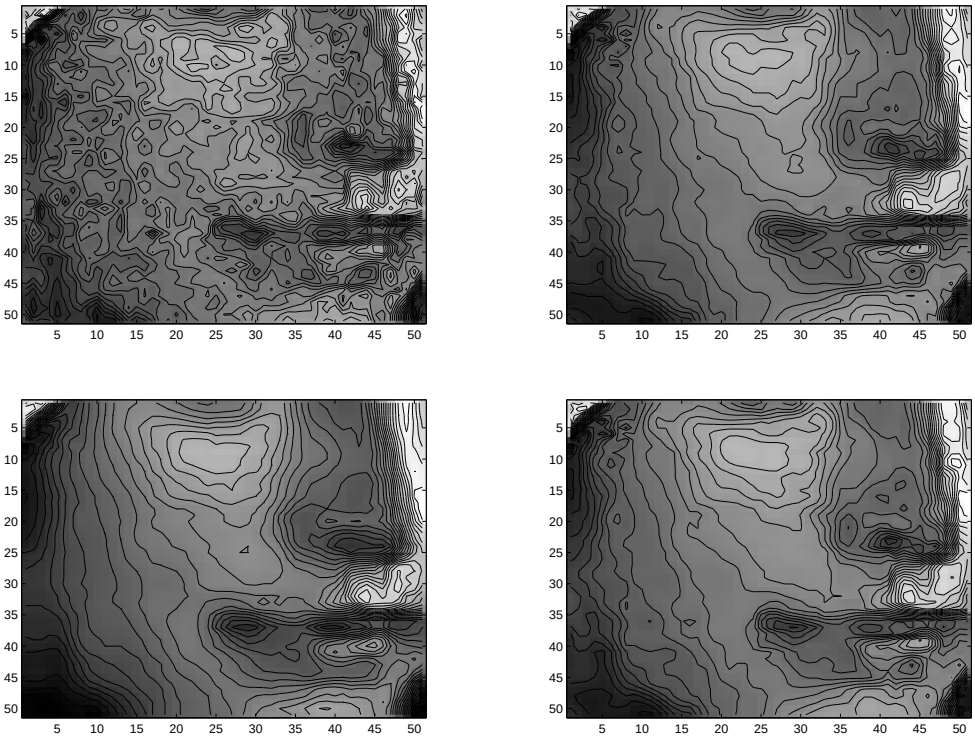

Figure 9: The plot of the contour for image of Lena face and $\sigma = 13$, SNRT$= 3.26$. Noising image (up left), restored image of model of the second-order equation (up right), restored image of model of the fourth-order equation (down left), and restored image of model of the compound equation (down right).

Table 5: Computational results for the image of Lena face and $\sigma = 13$, SNRT$= 3.26$.

Model	ε	N	Err2	Err0	CPU time
Equation of order 2	3.0^{-3}	6	7.25	38.04	0.09
Equation of order 4	$3*1.0^{-3}$	8	8.32	62.62	0.23
Compound equation	$3*1.0^{-3}$	7	6.58	45.23	0.18

Table 6: Computational results for the image of Lena face and $\sigma = 40$, SNRT$= 1.05$.

Model	ε	N	Err2	Err0	CPU time
Equation of order 2	$5*1.0^{-4}$	9	13.33	72.78	0.14
Equation of order 4	$5*1.0^{-4}$	31	13.21	65.59	0.79
Compound equation	$5*1.0^{-4}$	22	12.31	84.98	0.59

7.2.2. The image of Lena face with strong noise

Now, we consider a denoising problem with strong noise for the image of Lena face. The results and figures of the three models are in Table 6 and Fig. 10. The contour for recovered images of Lena face is presented in Fig. 11.

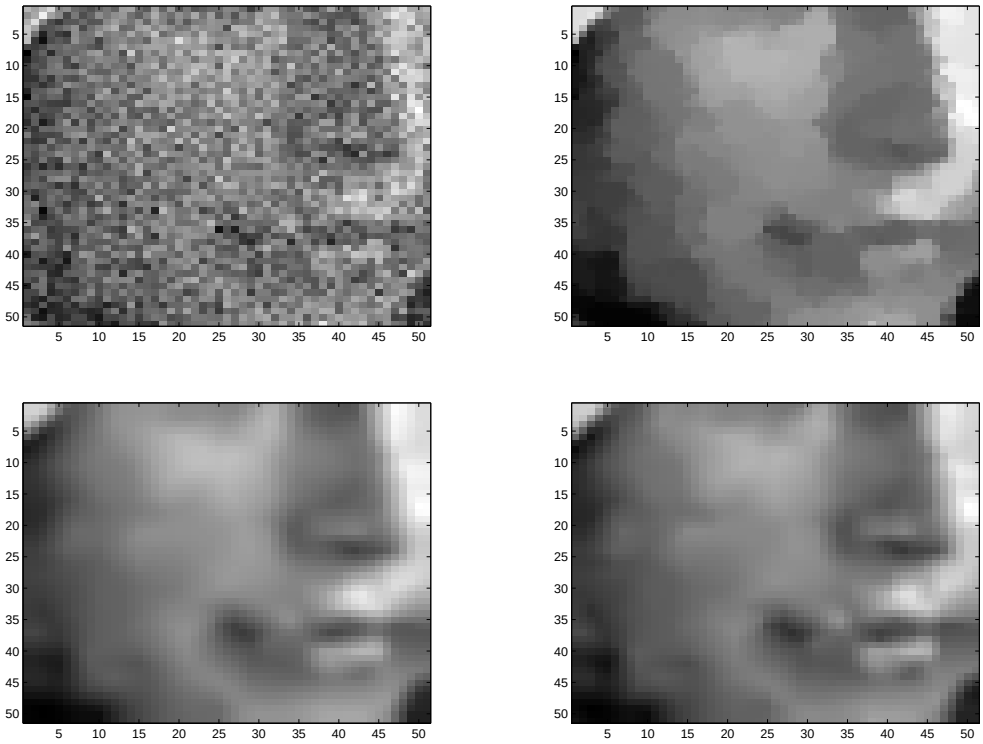

Figure 10: Noising image (up left), restored image of model of the second-order equation (up right), restored image of model of the fourth-order equation (down left), and restored image of model of the compound equation (down right) for the image of Lena face, and $\sigma = 40$, SNRT$= 1.05$.

From this example, we know that the denoising image is block-type for ROF model. The LLT model can keep smoothness of face very well and restored results are satisfactory. The restored image of the compound model is most closed original image. Especially, it is clear from the contour images at nose and left position that restored images of the compound model and the LLT model are good.

7.3. Image of squares and round

Now, we consider the denoising problems for the image of squares and round. Its original image is given in Fig. 12. The resolution of this image is 150*150.

7.3.1. The image of squares and round with weak noise

The image of squares and round with σ=10 has been considered in [14], p. 5. The results of the three models are given in Table 7 and Fig. 13.

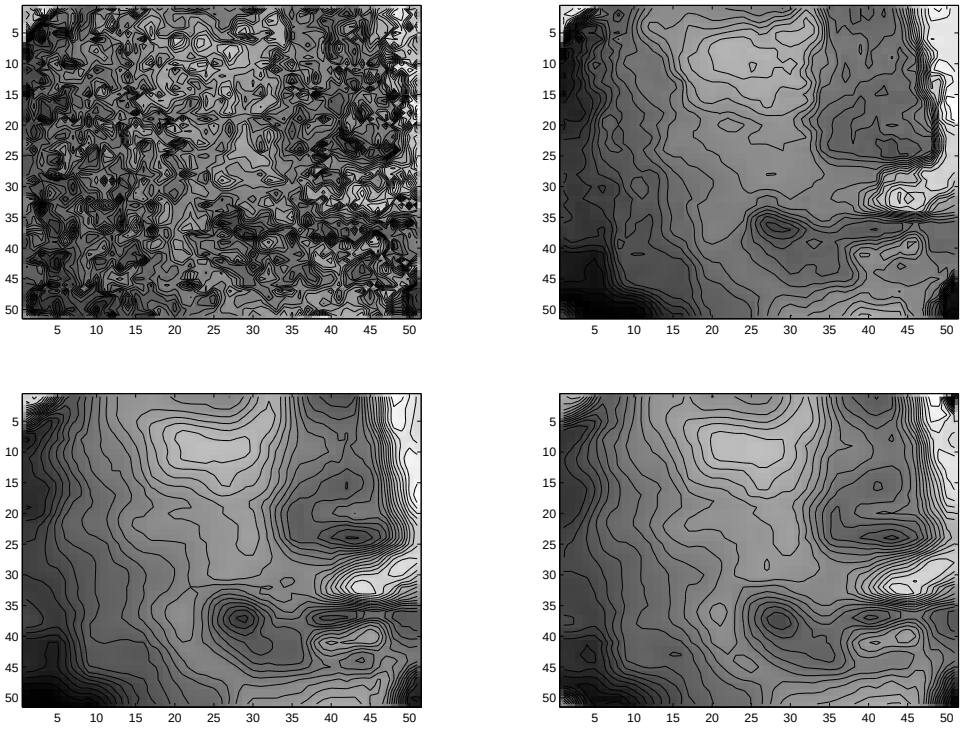

Figure 11: The plot of the contour for image of Lena face, and $\sigma = 40$, SNRT$= 1.05$. Noising image (up left), restored image of model of the second-order equation (up right), restored image of model of the fourth-order equation (down left), and restored image of model of the compound equation (down right).

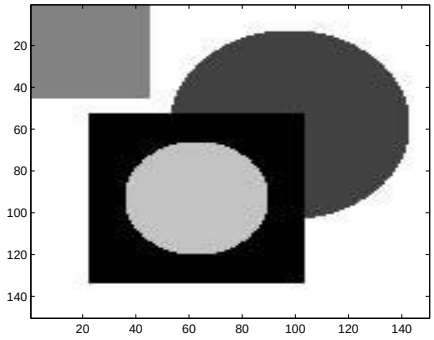

Figure 12: Original image of squares and round.

7.3.2. The image of squares and round with strong noise

The results of the three models are given in Table 8 and Fig. 14.

In this noising problem, we consider large variance σ=95. It is clear from previous

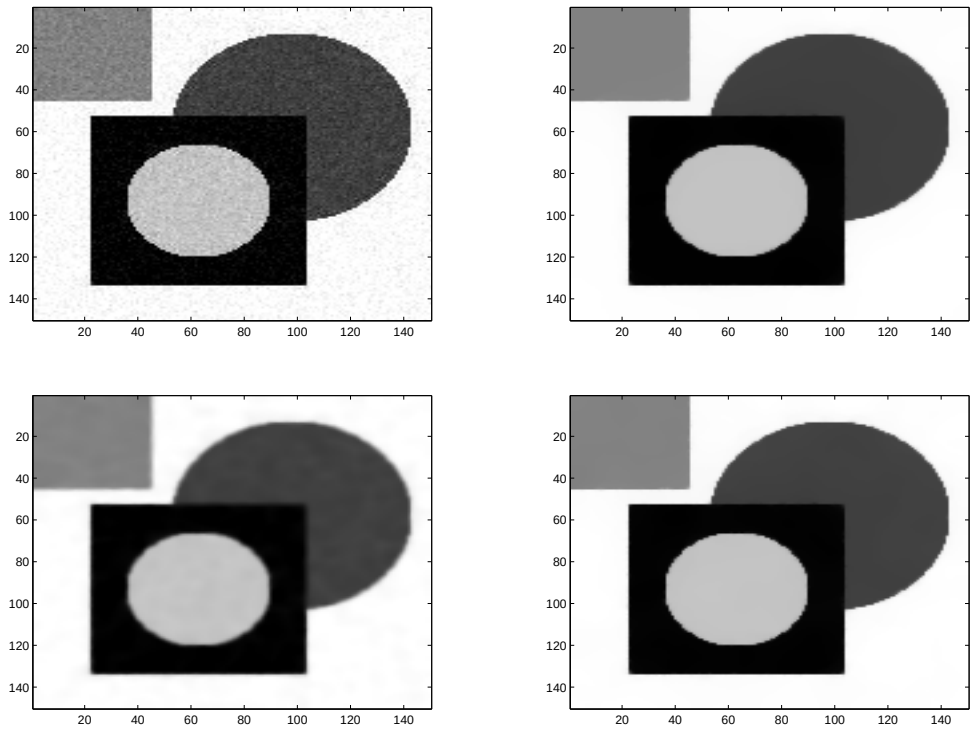

Figure 13: Noising image (up left), restored image of model of the second-order equation (up right), restored image of model of the fourth-order equation (down left), and restored image of model of the compound equation (down right) for the image of squares and round, and $\sigma = 10$, SNRT$= 10.28$.

Table 7: Computational results for the image of squares and round and $\sigma = 10$, SNRT$= 10.28$.

Model	ε	N	Err2	Err0	CPU time
Equation of order 2	1.0^{-3}	7	5.32	56.82	0.88
Equation of order 4	1.0^{-3}	9	11.85	98.92	2.14
Compound equation	1.0^{-3}	11	4.91	51.83	2.35

Table 8: Computational results for the image of squares and round and $\sigma = 95$, SNRT$= 1.08$.

Model	ε	N	Err2	Err0	CPU time
Equation of order 2	$5 * 1.0^{-4}$	8	22.06	200.96	1.06
Equation of order 4	$5 * 1.0^{-4}$	26	27.18	142.32	6.28
Compound equation	$5 * 1.0^{-4}$	10	17.60	189.58	1.85

results that the model of 4-th order equation has the smallest errors in L_∞ (i.e., "err0") and can keep shapes of small constructions in the images when noise is strong.

The compound algorithm is better than ROF model and model of LLT. The new compound algorithm can keep the small constructions and remove noise very well.

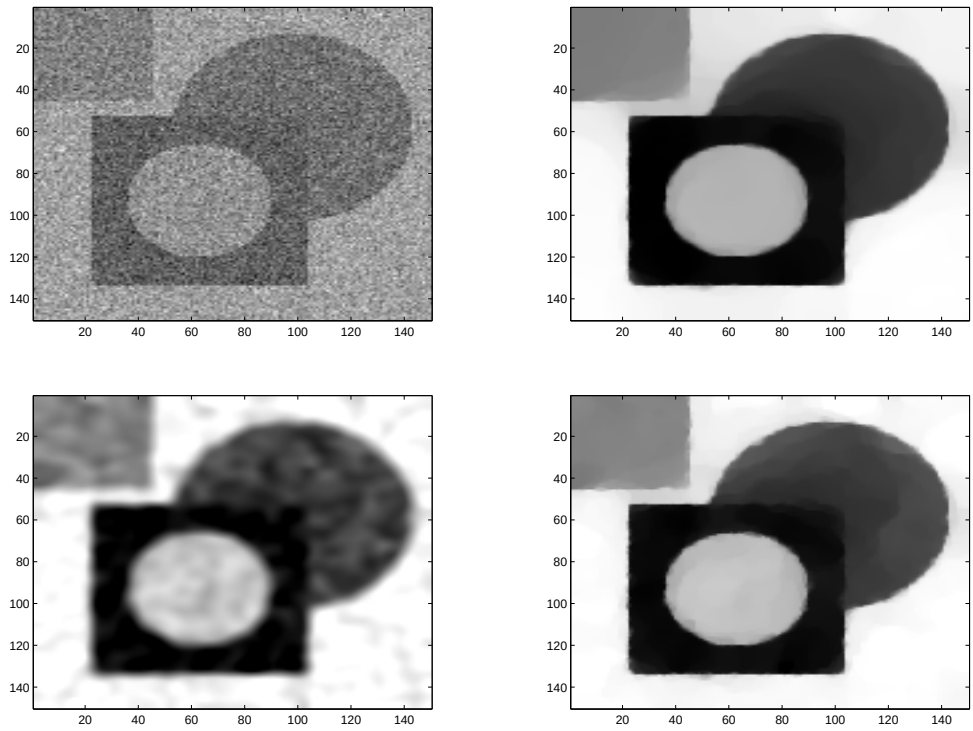

Figure 14: Noising image (up left), restored image of model of the second-order equation (up right), restored image of model of the fourth-order equation (down left), and restored image of model of the compound equation (down right) for the image of squares and round, and $\sigma = 95$, SNRT$= 1.08$.

8. Conclusion

The ROF model is a basic model for restoration problems, which can remove strong noise efficiently and keep edges very clearly. The CPU time of denoising for ROF model is the smallest in the three models.

We note from the tables that the errors of the LLT model in L_∞ are the smallest in the three models when noise is strong. The results demonstrate that the LLT model can handle smooth signals and keep small constructions and shapes of the images, especially, shapes of corners. From the figures, we know that the LLT model may remove noise and obtain satisfactory restorated images when the noise is weaker. For the Lena face images, the LLT model give smoother restored results.

In the compound model, the parameters $C_0 = 0$, and $C_d = 0.1$ are fixed. The parameter C_1 is dependent with discontinuity of the images and is taken as 30–255.

In conclusion, numerical experiments demonstrate that our compound algorithm is efficient and better than the models of the ROF and LLT for the noising images. The new algorithm preserves the main advantages of the ROF model and LLT model, in the sense that it can remove noise and keep small constructions and shapes of the images

very well. In all tables, the errors of the compound model between the exact images and corresponding restored images in L_2 norm are the smallest among the three models. For the denoising problems, the restored images of the compound algorithm are the best in the corresponding restored images.

Acknowledgments This work was initiated when Chang visited Nanyang Technological University of Singapore. Financial support from NSFC of China, Singapore NTU project SUG 20/07, MOE Grant T207B2202 and NRF2007IDMIDM002-010 are gratefully acknowledged here.

References

[1] R. Acar and C. R. Vogel, *Analysis of total variation penalty methods for ill-posed problems*, Inverse Problems, 10(1994), pp. 1217–1229.

[2] L. Alvarez, P.-L. Lions and J.-M. Morel, *Image selective smoothing and edge detection by nonlinear diffusion II*, SIAM J. Numer. Anal., 29(1992), pp. 845–866.

[3] C. A. Z. Barcelos and Y. Chen, *Heat flow and related minimization problem in image restoration*, Computers and Mathematics with Applications, 39(2000), No. 5-6, pp. 81–97.

[4] R. Chan, T. Chan and H. Zhou, *Advanced signal processing algorithms*, In proceedings of the International Society of Photo-Optical Instrumentation Engineers, F. Luk, ed., SPIE, 1995, pp. 314–325.

[5] T. F. Chan, G. H. Golub and P. Mulet, *A nonlinear primal-dual method for total variation-based image restoration*, SIAM J. Sci. Comput., 20(1999), pp. 1964–1977.

[6] T. F. Chan, A. Marquina and P. Mulet, *High-order total variation-based image restoration.*, SIAM J. Sci. Comput., 22(2000), pp. 503-516.

[7] Q. Chang and I. Chern, *Acceleration methods for total variation-based image denoising*, SIAM J. Sci. Comput., 25(2003), pp. 983–994.

[8] Q. Chang and Z. Huang, *Efficient algebraic multigrid algorithms and their convergence*, SIAM J. Sci. Comput., 24(2002), pp. 597–618.

[9] Q. Chang, S. Ma and G. Lei, *Algebraic multigrid method for queuing networks*, Int. J. of Computer Math., 70(1999), pp. 539–552.

[10] Q. Chang, Y. Wong and H. Fu, *On the algebraic multigrid method*, J. Comput. Phys., 125(1996), pp. 279–292.

[11] Q. Chang, W. C. Wang and J. Xu, *A method for total variation-based reconstruction of noisy and blurred images* in "Image Processing Based on Partial Differential Equations" (Eds. by X. Tai, K. Lie, T.F. Chan and S. Osher), Springer, 2006, pp. 92-108.

[12] A. Chambolle and P. L. Lions, *Image recovery via total variation minimization and related problems*, Numer. Math., 76(1997), pp. 167-188.

[13] M. Lysaker, A. lundervold and X. Tai, *Noise removal using forth-order partial differential equation with application to medical magnetic resonance images in space and time*, blurred images, IEEE Trans. Image Processing, 12(2003), pp. 1579-1590.

[14] Y. Lou, X. Zhang, S. Osher and A. Bertozzi, *Image recovery via nonlocal operation*, UCLA CAM report 06-35 Tech. Rep. 2008.

[15] M. Lysaker and X. Tai, *Iterative image restoration combining total variation minimization and a second-order functional*, Inter. J. of Compt. Vision, 66(2006), pp. 5-18.

[16] C. W. Oosterlee and T. Washio, *Krylov subspace acceleration of nonlinear multigrid with application to recirculating flows*, SIAM J. Sci. Comput., 21(2000), pp. 1670–1690.

[17] S. Osher and L. Rudin, *Feature-oriented image enhancement using shock filters*, SIAM J. Numer. Anal., 27(1990), pp. 919–940.
[18] L. Rudin, S. Osher and E. Fatemi, *Nonlinear total variation based noise removal algorithms*, Phys. D, 60(1992), pp. 259–268.
[19] J. Ruge and K. Stüben, *Algebraic multigrid, In Multigrid Methods*, (S. F. McCormick, ed.) 4, SIAM, Philadelphia, (1987), pp. 73–130.
[20] C. R. Vogel and M. E. Oman, *Iterative methods for total variation denoising*, SIAM J. Sci. Comput., 17(1996), pp. 227–238.
[21] C. R. Vogel and M. E. Oman, *Fast, robust total variation-based reconstruction of noisy*, blurred images, IEEE Trans. Image Processing, 7(1998), pp. 813–824.
[22] G. W. Wei, *Generalized Perona- Malik equation for image restoration*, IEEE Signal Processing Letters, 6(1999), pp. 165-167.
[23] Y. L. You and M. Kaveh, *Fourth-order partial differential equation for noise removal*, blurred images, IEEE Trans. Image Processing, 7(1998), pp. 813–824.